Robotica (2012) volume 30, pp. 379–388. © Cambridge University Press 2011
doi:10.1017/S026357471100066X

Backlash elimination in parallel manipulators using actuation redundancy

Roger Boudreau†,*, Xu Mao‡ and Ron Podhorodeski‡

†*Département de génie mécanique, Université de Moncton, Moncton, Nouveau-Brunswick, Canada*
‡*Robotics and Mechanisms (RAM) Laboratory, Department of Mechanical Engineering, University of Victoria, Victoria, British Columbia, Canada*

(Received in Final Form: June 10, 2011; accepted June 9, 2011. First published online: July 11, 2011)

SUMMARY
In this work, accuracy enhancement through backlash elimination is considered. When a nonredundantly actuated parallel manipulator is subjected to a wrench while following a trajectory, required actuator torque switching (going from positive to negative or vice versa) may occur. If backlash is present in the actuation hardware for a manipulator, torque switching compromises accuracy. When in-branch redundant actuation is added, a pseudoinverse torque solution requires smaller joint torques, but torque switching may still occur. A method is presented where concepts of exploiting a nullspace basis of the joint torques are used to ensure that single sense joint torques can be achieved for the actuated joints. The same sense torque solutions are obtained using nonlinear optimization. The methodology is applied to several examples simulating parallel manipulators in machining applications.

KEYWORDS: Actuation redundancy; Parallel manipulators; Backlash elimination; Optimization.

1. Introduction

Parallel manipulators (PMs) are being used for manufacturing tasks that require high precision. Clearances in mechanical joints induce backlash and can prevent a manipulator from performing at the desired level of accuracy. Monolithic flexure joints have been proposed to replace mechanically assembled joints that have inaccuracies due to manufacturing tolerances.[1–3]

Inaccuracies due to backlash are eliminated if there are no sign reversals in the control torques. Redundancy has been proposed as a means to ensure no sign reversals. Müller[4] and Müller and Maisser[5] considered additional branch redundant actuation (a planar 4-$\underline{RRR}^1$ PM and a spatial hexapod). They avoided backlash by considering internal preloading, Lagrangian motion equations, and inverse dynamics, allowing internal preload control. Müller considers nullspace basis vectors to control required joint torque senses. Wei and Simaan[6] proposed using preloaded springs at the wrist joints of a planar 3-$\underline{P}RR$ PM to eliminate backlash in the prismatic joints. The necessary torsional preloads are determined by formulating a Lagrange problem that minimizes the elastic energy of the robot.

Joint clearances in the passive joints also cause backlash. They can be an important source of error on the position and orientation accuracy of manipulators. Several methods have been proposed for modeling clearance to determine its effect on the performance of manipulators.[7–9] Backlash in passive joints is not considered here.

Within this work, in-branch actuation redundancy is utilized to eliminate backlash created inaccuracies at the actuated joints of a planar PM. In particular, the 3-branch (3-$\underline{R}RR$) manipulator considered by Gosselin and Angeles[10] is in-branch redundantly actuated resulting in a 3-$\underline{RR}R$ PM. While requiring the actuation of the elbow joints of the device, the actuation of the elbow joints reduces the joint torques of the branch 1st joints (base joints) requiring smaller actuators.

Redundancy in PM components has been considered by numerous researchers. There are several forms of this redundancy. Redundant in-branch actuation[11] and redundant additional branch actuation[12] have been investigated for the elimination of PM force unconstrained configurations. Zibil *et al.*[13] considered analytical methods for determining force moment capabilities of redundantly actuated planar PMs. Kinematically redundant branches[14] have been considered to enhance workspaces and eliminate singularities of PMs. Merlet[15] considers the advantages of PMs with redundant actuation.

In this current work, screw coordinate matrices of the associated reciprocal screws (ARSs) are used to model the force capabilities of PMs. Nullspace basis vectors of the ARS matrices, and their multipliers, are used to allow elbow joint torque-based compensation. Nonlinear optimization is used to ensure nonreversing signs of the actuated torques. Section 2 presents a description of the manipulator used in this study. Section 3 presents some background on ARSs, leading to the formulation of the torque solutions for the nonredundant and the redundant manipulators in Sections 4 and 5, respectively. Section 5 also presents the nullspace basis determination and the proposed method to obtain nonreversing signs for the actuation torques of the redundant manipulator. Section 6 presents the results simulating the manipulator in machining applications. It is assumed that

* Corresponding author. E-mail: roger.a.boudreau@umoncton.ca
[1] Within the PM descriptions, the preceding number indicates the number of branches, *R* denotes a revolute joint, *P* a prismatic joint and the underline indicates the actuated joint(s).

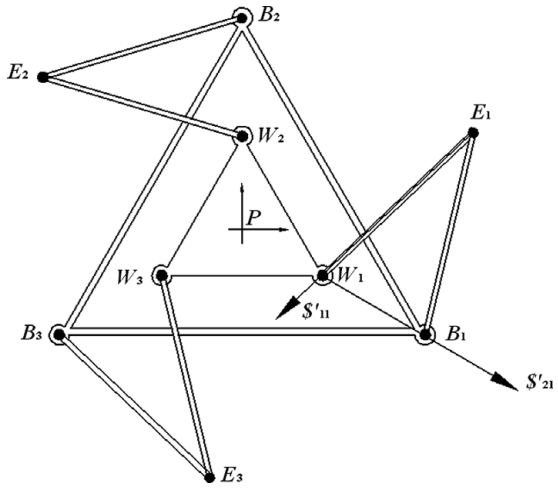

Fig. 1. 3-RRR manipulator, platform and base attachment points, and associated reciprocal screws.

motion is slow, allowing a kinetostatic analysis. A discussion and a conclusion follow. Within the work presented in this paper, concepts of screw theory are utilized. For knowledge beyond the work presented in this paper, the reader is referred to Ball[16] and Hunt.[17]

2. Manipulator Description

Figure 1 depicts a symmetrical 3-*RRR* PM with associated labeling including B_j, E_j, and W_j being the base, elbow, and wrist joints of the jth branch, $j = 1, 2$, and 3. Appendix A presents an inverse displacement solution for the 3-*RRR* PM.

In Fig. 1, $\$'_{11}$ and $\$'_{21}$ denote the ARSs for the 1st and 2nd (base and elbow) actuated joints of branch 1. Similar ARSs exist for the actuated joints of branches 2 and 3. ARSs are reciprocal to all joints in a branch except the actuated joint to which it is associated. Since only revolute joints are present in this manipulator, and hence to be reciprocal, the ARS of an actuated joint passes through the other two joints of the branch.

Within Fig. 1, a frame $\{\mathbf{p}\}$ is fixed to the platform and has an origin p coincident with the payload platform center. The orientation of $\{\mathbf{p}\}$ is defined by $\boldsymbol{X}_p$ being in the direction parallel to a line from W_3 to W_1, and $\boldsymbol{Y}_p$ being defined by the location of W_2. The fixed base frame $\{\mathbf{b}\}$ is located at the geometrical center of the base joints.

3. Expressing Force Problems with Associated Reciprocal Wrenches and Joint Torques (Wrench Intensities)

Assume ${}^p\boldsymbol{F} = {}^p\{f_x, f_y; m_{zp}\}^{\mathrm{T}} = {}^p\{\boldsymbol{f}; m_{zp}\}^{\mathrm{T}}$ is a wrench composed of a force and moment to be applied by the manipulator known with respect to (wrt) $\{\mathbf{p}\}$. ${}^p\boldsymbol{F}$ has force components ${}^p\boldsymbol{f} = {}^p\{f_x, f_y\}^{\mathrm{T}}$ in the x- and y-directions and a moment m_{zp} that is about the point p and is only about the z-direction. From ${}^p\boldsymbol{F}$, a wrench ${}^b\boldsymbol{F}$ wrt $\{\mathbf{b}\}$ can be found, i.e.,

$$ {}^b\boldsymbol{F} = \left\{ {}^b_p\boldsymbol{R}^p\boldsymbol{f}; m_{zp} + {}^b\boldsymbol{r}_{b-p} \times {}^b_p\boldsymbol{R}^{\mathrm{p}}\boldsymbol{f} \right\}. \tag{1} $$

In Eq. (1), ${}^b_p\boldsymbol{R}$ is a rotation matrix describing the orientation of $\{\mathbf{p}\}$ wrt $\{\mathbf{b}\}$[18]; the position vector ${}^b\boldsymbol{r}_{b-p}$ describes the location of the origin of $\{\mathbf{p}\}$ wrt the origin of $\{\mathbf{b}\}$ in terms of $\{\mathbf{b}\}$'s orientation; and "$\times$" denotes a vector cross product. Note that since a planar manipulator is being considered ${}^b\boldsymbol{r}_{b-p} \times {}^b_p\boldsymbol{R}^{\mathrm{p}}\boldsymbol{f}$ will be in the z-direction.

The wrench ${}^b\boldsymbol{F}$ can also be expressed in terms of wrench intensities, w_{ij}, and the ARSs, $\$'_{ij}$, of the actuated joints. That is,

$$ {}^b\boldsymbol{F} = \sum_j \sum_i {}^b\$'_{ij} w_{ij}, \quad i = 1, nb_j, \ j = 1, nb, \tag{2} $$

where nb_j is the number of actuated joints in branch j, and nb is the number of branches. ${}^b\$'_{ij}$ is reciprocal to the joints other than joint i in branch j. Appendix B summarizes the ARSs of the 3-*RRR* and 3-*RRR* PMs wrt $\{\mathbf{b}\}$.

The wrench intensity required of the ith actuated joint of branch j is w_{ij}. The required joint torque τ_{ij} in terms of w_{ij}, ${}^b\$'_{ij}$, and ${}^b\$_{ij}$ is

$$ \tau_{ij} = w_{ij} \left({}^b\$'_{ij} \circledast {}^b\$_{ij} \right), \tag{3} $$

where ${}^b\$_{ij}$ are the screw coordinates of the ith actuated joint of branch j and $\circledast$ indicates a reciprocal product, i.e.,

$$ \begin{aligned} &\text{if } \boldsymbol{F} = \{\boldsymbol{f}; \boldsymbol{m}\}^{\mathrm{T}} = \{f_x, f_y; m_z\}^{\mathrm{T}} \quad \text{and} \\ &\quad \boldsymbol{V} = \{\boldsymbol{\omega}; \mathbf{v}\}^{\mathrm{T}} = \{\omega_z; \mathrm{v}_x, \mathrm{v}_y\}^{\mathrm{T}}, \\ &\boldsymbol{F} \circledast \boldsymbol{V} = \boldsymbol{f} \cdot \mathbf{v} + \boldsymbol{m} \cdot \boldsymbol{\omega} = f_x \mathrm{v}_{\mathrm{x}} + f_y \mathrm{v}_{\mathrm{y}} + m_z \omega_{\mathrm{z}}. \end{aligned} \tag{4} $$

Within Eq. (3), $({}^b\$'_{ij} \circledast {}^b\$_{ij})$ is related to the mechanical advantage of the ith actuated joint of branch j. It represents the perpendicular distance between ${}^b\$'_{ij}$ and ${}^b\$_{ij}$.

4. Static Force Problem for the 3-*RRR* and 3-*RRR* Manipulators

In terms of ARSs and wrench intensities, the wrench for a 3-*RRR* PM can be expressed as

$$ {}^b\boldsymbol{F} = {}^b[\$'_{11}\$'_{12}\$'_{13}]\{w_{11}, w_{12}, w_{13}\}^{\mathrm{T}} = {}^b[\$'_3]\{\mathbf{w}_3\}. \tag{5} $$

The screw coordinates for the ARSs $\$'_{11}$, $\$'_{12}$, and $\$'_{13}$ for the actuated base joints B_j are given in Appendix B and have been grouped in a matrix ${}^b[\$'_3]$ in Eq. (5). The joint torques τ_{ij} are equal to the wrench intensities multiplied by a mechanical advantage weighting factor, as in Eq. (3). A similar equation using the ARSs and wrench intensities for the elbow joints can be written for the 3-*RRR* PM. The screw coordinates of the ARSs $\$'_{21}$, $\$'_{22}$, and $\$'_{23}$ for the actuated elbow joints E_j are also given in Appendix B.

The matrix ${}^b[\$'_3]$ in Eq. (5) is due to three actuated joints, is square (3×3), and the above static force problem can be solved for the required $\{\mathbf{w}_3\}$ values (a 3×1 vector) for a given wrench by inversion of ${}^b[\$'_3]$ or another linear algebra technique[19], i.e.,

$$ \{\mathbf{w}_3\} = {}^b[\$'_3]^{-1\,b}\boldsymbol{F}, \tag{6} $$

https://doi.org/10.1017/S026357471100066X Published online by Cambridge University Press

where ${}^b\boldsymbol{F}$ is the wrench applied by the manipulator. The joint wrench intensities $\{\mathbf{w}_3\}$ can be converted into corresponding τ_{ij} using Eq. (3). For a 3-*RRR* manipulator with the second joint actuated, an equation similar to Eq. (6) can be used to solve the static force problem where the ARSs of the second actuated joints are used in $[\$'_3]$.

5. Required Input Torques for a 3-*RRR* Manipulator

5.1. Static force problem

In the case of the redundantly actuated 3-*RRR* PM, $nb = 3$, and two joints (base and elbow) are actuated per branch. In terms of ARSs, wrench intensities and the force to be applied, the static force problem can be expressed by

$$\begin{aligned}{}^b\boldsymbol{F} &= {}^b[\$'_{11}\$'_{12}\$'_{13}\$'_{21}\$'_{22}\$'_{23}]\{w_{11}, w_{12}, w_{13}, w_{21}, w_{22}, w_{23}\}^{\mathrm{T}}\\ &= {}^b[\$'_6]\{\mathbf{w}_6\}. \end{aligned} \tag{7}$$

Matrix $[\$'_6]$ is due to six actuated joints and is of dimension 3×6. There are three dimensions of solutions for the six elements of $\{\mathbf{w}_6\}$. Within robotics it is often suggested to use the right Moore–Penrose pseudoinverse[19] of the Jacobian matrix for joint redundant serial manipulators. A pseudoinverse of $[\$'_6]$ could be considered, yielding

$$\{\mathbf{w}_6\} = {}^b[\$'_6]^{+b}\boldsymbol{F}, \tag{8}$$

where $[\$'_6]^+ = [\$'_6]^{\mathrm{T}}(([\$'_6][\$'_6])^{\mathrm{T}})^{-1}$. Note that a Moore–Penrose pseudoinverse solution returns a solution with a minimum 2-norm[19] of the elements of $\{\mathbf{w}_6\}$.

5.2. Nullspace basis vectors for ${}^b[\$'_6]$

A single sense solution for the elements of $\{\mathbf{w}_6\}$ can be achieved by exploiting a nullspace basis of $[\$'_6]$. One approach for finding a nullspace basis for $[\$'_6]$ is to find basis vectors by first resolving magnitudes required to produce $\$'_{21}, \$'_{22}$, and $\$'_{23}$ using the screw quantities of $[\$'_3]$. Consider the vectors $\boldsymbol{v}_j$ that satisfy the following relation:

$$[\$'_3]\{\boldsymbol{v}_j\} + \$'_{2j} = 0 \quad \text{or} \quad \{\boldsymbol{v}_j\}_{3\times1} = [\$'_3]^{-1}(-\$'_{2j}), \qquad j = 1, 2, 3. \tag{9}$$

Three nullspace basis vectors for $[\$'_6]$ can be assembled as

$$\{\boldsymbol{V}_1\}_{6\times1} = \{\{\boldsymbol{v}_1\}^{\mathrm{T}}, 1, 0, 0\}^{\mathrm{T}}, \tag{10a}$$

$$\{\boldsymbol{V}_2\}_{6\times1} = \{\{\boldsymbol{v}_2\}^{\mathrm{T}}, 0, 1, 0\}^{\mathrm{T}}, \tag{10b}$$

$$\{\boldsymbol{V}_3\}_{6\times1} = \{\{\boldsymbol{v}_3\}^{\mathrm{T}}, 0, 0, 1\}^{\mathrm{T}}. \tag{10c}$$

Note that

$$[\$'_6]_{3\times6}[\boldsymbol{V}_1\boldsymbol{V}_2\boldsymbol{V}_3]_{6\times3} = [\mathbf{0}]_{3\times3}, \tag{11}$$

i.e., the vectors $\{\boldsymbol{V}_j\}$, $j = 1, 2, 3$, form a nullspace basis of $[\$'_6]$. Wrench intensities based on multiples of the nullspace vectors cause forces internal to the PM.

A wrench intensity solution for the 3-*RRR* can be expressed as

$$\{\boldsymbol{w}\}_{6\times1} = \{\boldsymbol{w}_p\}_{6\times1} + \{\boldsymbol{w}_h\}_{6\times1}. \tag{12}$$

In Eq. (12), $\{\boldsymbol{w}_p\}$ is a particular $\{\boldsymbol{w}\}$ solution that produces the desired wrench ${}^bF$. Also in Eq. (12), $\{\boldsymbol{w}_h\}$ is a homogeneous torque solution that lies in the nullspace of $[\$'_6]$. Specifically, for the chosen nullspace vectors

$$\{\boldsymbol{w}_h\}_{6\times1} = [\boldsymbol{V}_1\boldsymbol{V}_2\boldsymbol{V}_3]_{6\times3}\{w_{21}, w_{22}, w_{23}\}^{\mathrm{T}}_{3\times1}, \tag{13}$$

i.e., the solution for $\{\boldsymbol{w}_h\}$ is dependent on the values chosen for w_{21}, w_{22}, w_{23}.

5.3. Values for w_{21}, w_{22}, and w_{23} to ensure desired w_{11}, w_{12}, and w_{13} values

To ensure specific (and therefore single sense) w_{11}, w_{12}, and w_{13}, let w_{11d}, w_{12d}, and w_{13d} be the desired values for w_{11}, w_{12}, and w_{13}. Assume that particular values for w_{11p}, w_{12p}, and w_{13p} have been found from

$$\{\boldsymbol{w}_p\} = \{w_{11p}, w_{12p}, w_{13p}\}^{\mathrm{T}} = {}^b[\$'_3]^{-1\,b}\boldsymbol{F}. \tag{14}$$

The difference $(\{\boldsymbol{w}\}_{df})$ between the desired values and the particular values found in (14) is given by

$$\{\boldsymbol{w}\}_{df} = \{w_{11df}, w_{12df}, w_{13df}\}^{\mathrm{T}} = \{w_{11d}, w_{12d}, w_{13d}\}^{\mathrm{T}} - \{w_{11p}, w_{12p}, w_{13p}\}^{\mathrm{T}}. \tag{15}$$

The elbow wrench intensities $\{w_{21c}, w_{22c}, w_{23c}\}^{\mathrm{T}}$ that will generate $\{\mathbf{w}\}_h$ that compensates for $\{w_{11df}, w_{12df}, w_{13df}\}^{\mathrm{T}}$ are

$$\{w_{21c}, w_{22c}, w_{23c}\}^{\mathrm{T}} = [\{\boldsymbol{v}_1\}\{\boldsymbol{v}_2\}\{\boldsymbol{v}_3\}]^{-1}\{w_{11df}, w_{12df}, w_{13df}\}^{\mathrm{T}}. \tag{16}$$

The following equation shows that any desired $\{\boldsymbol{w}_d\} = \{w_{11d}, w_{12d}, w_{13d}\}^{\mathrm{T}}$ wrench intensities for the first joint found by summing a homogeneous solution based on $\{w_{21c}, w_{22c}, w_{23c}\}^{\mathrm{T}}$ with the particular solution of Eq. (14) produces the correct intensities.

$$\begin{aligned}\{w_{11d}, w_{12d}, w_{13d}\}^{\mathrm{T}} &= {}^b[\$'_3]^{-1b}\boldsymbol{F}\\ &\quad + [\boldsymbol{v}_1\boldsymbol{v}_2\boldsymbol{v}_3]\{w_{21c}, w_{22c}, w_{23c}\}^{\mathrm{T}},\\ &= \{\boldsymbol{w}_p\} + \{w_{11df}, w_{12df}, w_{13df}\}^{\mathrm{T}}\\ &= \{\boldsymbol{w}_p\} + \{\{\boldsymbol{w}_d\} - \{\boldsymbol{w}_p\}\} = \{\boldsymbol{w}_d\}. \end{aligned} \tag{17}$$

For the problem at hand, same sense torques are desired for all the actuated joints.

5.4. Method for ensuring nonreversing torque values

It is desired to find backlash-free torques to follow a trajectory while the manipulator is subjected to a certain wrench. Note that the following discussion is in terms of wrench intensities but it is also valid for torques since the conversion is easily obtained with Eq. (3). It is possible to impose desired nonreversing wrench intensities for the base joints. Elbow wrench intensities can then be computed using Eq. (16) for those desired values. To ensure that the computed elbow wrench intensities do not change sign, the solution was formulated as a

https://doi.org/10.1017/S026357471100066X Published online by Cambridge University Press

constrained nonlinear optimization problem. The multiplicity of solutions to the inverse static force problem for a redundant manipulator allows the minimization of an objective function (OF) such that $OF = \sum_{i=1}^{n} L$ along a trajectory divided into n discrete points. The cost function was chosen here as $L = \boldsymbol{\tau}^{\mathrm{T}}\boldsymbol{\tau}$, where $\boldsymbol{\tau}$ represents the vector of actuated joint torques. The method is summarized as follows:

(a) Specify a function that does not change sign for the base joint wrench intensities, i.e., desired values w_{1jd}, $j = 1, 2, 3$. The parameters that define the function are the search variables for the optimization. Then, at each step of the trajectory:
  (i) Compute the ARS of each actuated joint;
  (ii) Compute the nullspace vectors $\{\boldsymbol{v}_j\}^{\mathrm{T}}$using Eq. (9);
  (iii) Calculate a particular wrench intensity $\{\mathrm{w}_{11\mathrm{p}}, \mathrm{w}_{12\mathrm{p}}, \mathrm{w}_{13\mathrm{p}}\}^{\mathrm{T}}$ solution using Eq. (14);
  (iv) Calculate the vector $\{w_{11df}, w_{12df}, w_{13df}\}^{\mathrm{T}}$ containing the difference between the desired wrench intensity at the base joints $\{w_{11d}, w_{12d}, w_{13d}\}^{\mathrm{T}}$ and the particular solution $\{\mathrm{w}_{11\mathrm{p}}, \mathrm{w}_{12\mathrm{p}}, \mathrm{w}_{13\mathrm{p}}\}^{\mathrm{T}}$ using Eq. (15);
  (v) Resolve $\{w_{21c}, w_{22c}, w_{23c}\}^{\mathrm{T}}$ using Eq. (16) to determine the elbow joint wrench intensities required to compensate for the difference;
  (vi) Convert the wrench intensities into joint torques using Eq. (3);

(b) Stop when the nth step in the trajectory has been reached;
(c) Compute the OF such that $L = \sum \boldsymbol{\tau}^{\mathrm{T}}\boldsymbol{\tau}$.

The problem was solved using a constrained nonlinear optimization algorithm called *fmincon* found in Matlab's optimization toolbox. This function uses a sequential quadratic programming method. Nonreversing signs of the computed elbow torques were added as constraints in the optimization routine.

6. Implementation and Results

6.1. Trajectories

Three examples are presented. In all examples, the manipulator is considered to be used in a machining operation following a given trajectory. It is assumed that motion is very slow along the trajectory so that dynamic effects are negligible and a kinetostatic analysis is justified. The trajectories were chosen such as to generate torques that switch directions when a nonredundant manipulator is used. A 100 N force is considered to be acting on the manipulator in the direction opposite to its motion, i.e., tangent to its trajectory. No moment is considered to be applied on the platform. However, from Eq. (1), it can be seen that a moment will be applied wrt $\{\mathbf{b}\}$. The orientation of the platform is constant at $\pi/6$ rad.

The first trajectory considered is a circle centered at (0.1, 0.1) m with a radius of 0.05 m. The wrench applied by the manipulator in frame $\{\mathbf{b}\}$ will be

$$^{b}\boldsymbol{F} = {}^{b}\{f_x, f_y; m_z\}^{\mathrm{T}} = \{-100\sin\theta, 100\cos\theta; -yf_x + xf_y\}^{\mathrm{T}}\ \mathrm{N};\ \mathrm{Nm}, \quad (18)$$

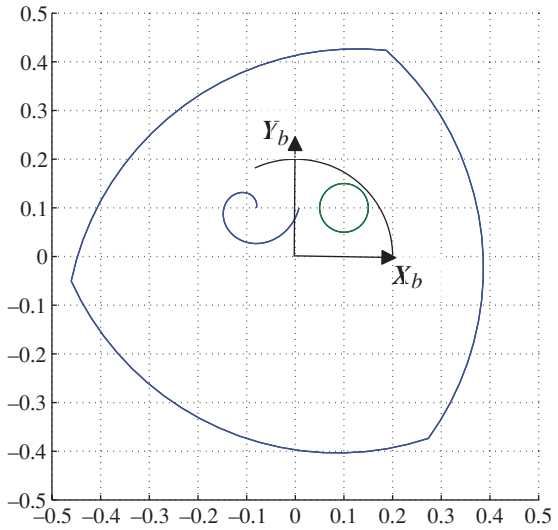

Fig. 2. (Colour online) Constant orientation workspace and trajectories.

where θ is the angle between the horizontal line passing through the center of the circle and the radius to a point on the circle, and x and y are the coordinates of a point on the circle.

The second trajectory is a logarithmic spiral described by the following polar equation[20]:

$$\rho = ae^{k\beta} \quad \text{with} \quad k = \cot\psi, \quad (19)$$

where ρ is the spiral radius for a given angle β, a is a constant (set here at 0.02 m), and ψ is the angle between the tangent and radial line at the polar point (ρ, β). Angle ψ is chosen as 75°, and the center of the spiral is at $(-0.1, 0.1)$ m. The wrench applied by the manipulator in this case is then

$$^{b}\boldsymbol{F} = {}^{b}\{f_x, f_y; m_z\}^{\mathrm{T}} = \{100\cos(\beta+\psi), 100\sin(\beta+\psi); -yf_x + xf_y\}^{\mathrm{T}}\ \mathrm{N};\ \mathrm{Nm}, \quad (20)$$

where β varies in this example from 0 to 2π, and x and y are the coordinates of a point on the spiral.

The third trajectory is an arc of radius $r = 0.2$ m, centered at the origin, and limited by the horizontal axis and an angle of 2 rad (114.6°). This trajectory was chosen because it contains a position that is very close to a singularity when considering the ARSs of the base actuated joints. The wrench is again defined by Eq. (18).

Three manipulators are considered, the nonredundantly actuated 3-*RRR* PM and 3-*RRR* PM, where one joint is actuated in each branch, and the redundantly actuated 3-*RRR* PM with two joints actuated in each branch. The PMs all have length dimensions of 0.3 m for each arm segment and for each edge of the common platform. The base platform for the example has edge dimensions of 0.6 m.

Figure 2 shows the constant orientation workspace ($\phi = \pi/6$) obtained using a geometrical method[21] of a 3-*RRR* manipulator with the above dimensions. The assembly mode shown in the Fig. 1 is used in all results. Also shown in the figure are the circle, the spiral, and the arc trajectories.

https://doi.org/10.1017/S026357471100066X Published online by Cambridge University Press

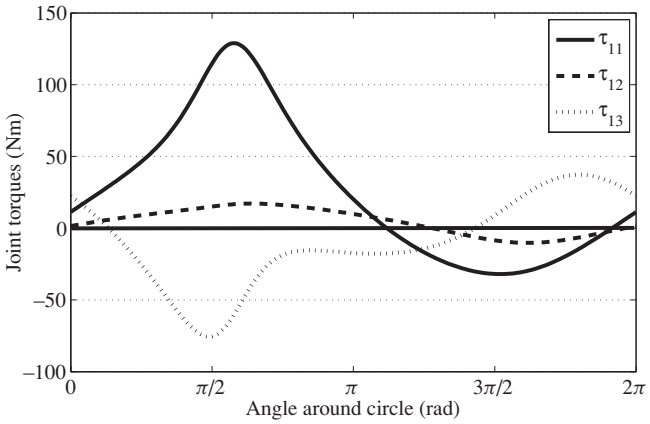

Fig. 3. 3-*RRR* manipulator joint torques to follow circle trajectory.

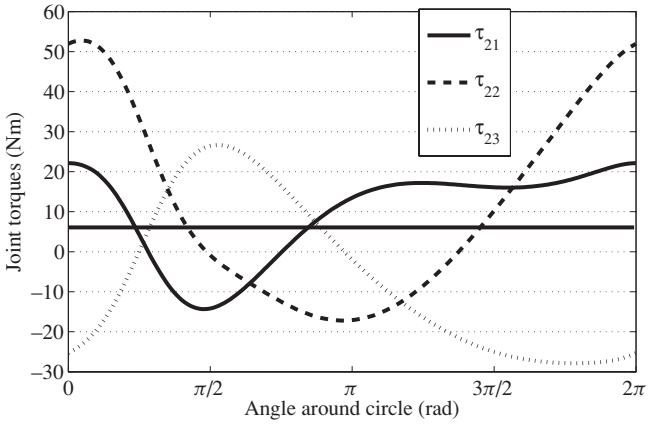

Fig. 4. 3-*RRR* manipulator joint torques to follow circle trajectory.

6.2. *Nonredundantly actuated PMs (circle trajectory)*

The first results presented are for the circle trajectory with the two nonredundantly actuated PMs. Illustrated in Fig. 3 are the required torques τ_{11}, τ_{12}, and τ_{13} for the 3-*RRR* PM with the wrench of Eq. (18). Notice that the required torques have sign reversals (sometimes they are positive and sometimes they are negative depending on the position). As mentioned previously, when a joint torque value changes sign, if there is any backlash present in the system used to transmit the torque to the joint, a negative impact on the accuracy of the PM will be present.

The resulting elbow torques necessary to follow the circle trajectory for the 3-*RRR* PM are shown in Fig. 4. Again, sign reversals are observed for the joint torque values.

6.3. *Pseudoinverse solution for the 3-RRR PM (circle trajectory)*

Figure 5 illustrates the required joint torques considering the Moore–Penrose pseudoinverse solution and the wrench intensity to joint torque conversion of Eq. (3). The solution does not ensure that the joint torques are of a single sense, i.e., the goal of this work.

6.4. *Optimization solution for the 3-RRR PM (circle trajectory)*

As outlined in Section 5.4, the first step is to specify functions for the desired base joint wrench intensities. To avoid backlash, these functions should not have sign reversals. It can be seen in Fig. 5 that the torques obtained with the pseudoinverse solution are similar to sine waves. Because of this, and also due to the simplicity in specifying this function's sign, it was decided to use sine waves as functions for the desired wrenches of the base joints. To ensure that they do not change sign, the following was used for w_{1jd}, $j = 1, 2, 3$:

$$w_{1jd} = \overline{w_j} + \alpha_j \overline{w_j} \sin(\theta + \gamma_j) \; j = 1, 2, 3, \qquad (21)$$

where $\overline{w_j}$, α_j, and γ_j are the mean value, a factor setting the amplitude, and the phase angle, respectively, for the base joint desired wrench intensity values of branch j. Note that if values of α_j are limited to values between 0 and less than 1, the resulting sine wave will never change sign. The search space thus consists of nine variables, the three values introduced in Eq. (21) for each of the three branches. The optimization algorithm searches for these variables with a constraint that the joint wrench intensities of the elbow joints that are computed in steps (a)(i) through (a)(vi) of Section 5.4 do not change signs.

The trajectory was divided into 200 intervals to produce 201 points where the steps (a)(i) through (a)(vi) of Section 5.4 are computed. In the optimization algorithm, the following

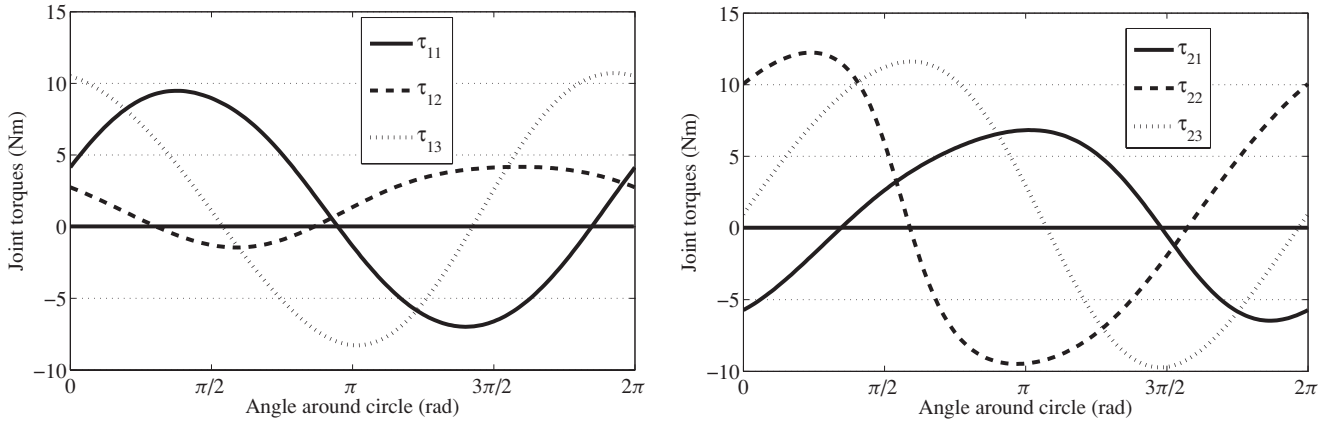

Fig. 5. 3-*RRR* manipulator joint torques to follow circle trajectory using the pseudoinverse solution: (a) Base (1st) joint torques; (b) Elbow (2nd) joint torques.

https://doi.org/10.1017/S026357471100066X Published online by Cambridge University Press

Table I. Optimization results, circle trajectory.

Combination	+++	++−	+−+	+−−	−++	−+−	−−+	−−−
OF/n_{points} (Nm)	802	779	DNC[a]	7831	1180	1524	DNC	1333
$\lvert\bar{\tau}\rvert$ (Nm)	11.6	11.4	–	36.1	14.0	15.9	–	47.1

[a]DNC = Did Not Converge.

bounds were used for the search terms that appear in Eq. (21):

$$\begin{aligned} 5 \le \overline{w_j} \le 100, \\ 0.1 \le \alpha_j \le 0.9, \\ 0 \le \gamma_j \le \pi. \end{aligned} \tag{22}$$

Note that when negative desired joint wrench intensities were specified, the mean value was bounded by $-100 \le \overline{w_j} \le -5$.

Eight (2^3) different combinations of signs are possible for the desired wrench intensities of the three base joints (+++, ++−, +−+,+−−, −++, −+−, −−+, −−−). All combinations were tested to find an optimized solution. Two of the combinations did not converge to a solution, and for the six combinations that were able to satisfy the constraints of same sense elbow torques, some performed better than others. The results obtained are sensitive to the initial input vector of the search variables. For combinations that did not converge, different initial vectors were tried to no avail. The results obtained are not necessarily a global optimum solution, but they nevertheless guarantee the elimination of backlash when following the trajectory. Table I presents the optimization results for all the combinations tested. The OF was divided by the number of points to report the average sum of torques squared for the trajectory. By dividing this value by the number of actuated joints, i.e., 6, and taking the square root, we obtain the average absolute value of the torques $|\bar{\tau}|$ along the trajectory.

Table I shows that some combinations have a better performance than others. Figure 6 presents the joint torques obtained after optimization with the ++− combination for the base joints to follow the circle trajectory that produced the smallest value for the OF. Note that none of the joint torques change sign.

For this trajectory, a comparison of Figs. 5 and 6 indicates that an increase in the magnitudes of the joint torques is required when ensuring same sense torque signs. For illustration purposes, results obtained with the −+− combination for the base joints, which produced an OF slightly larger in magnitude than that of the ++− combination, are shown in Fig. 7.

6.5. Spiral trajectory results

For the spiral trajectory described by Eq. (19) and for the applied wrench of Eq. (20), the nonredundantly actuated manipulators require reversing torques at each joint (curves not shown). The pseudoinverse solution for the actuated torques is shown in Fig. 8.

Due to the reasons explained in Section 6.4, the desired base joint wrench intensities were again modeled using Eq. (21), and the bounds in Eq. (22) were again used. The eight possible combinations of the signs of the desired wrench intensities were tested and are reported in Table II.

Figure 9 illustrates the joint torques obtained after optimization with the combination −−+ for the base joints signs that produced the smallest value for the OF to follow the spiral trajectory. Note that in Fig. 9(a), the desired sine

Table II. Optimization results, spiral trajectory.

Combination	+++	++−	+−+	+−−	−++	−+−	−−+	−−−
OF/n_{points} (Nm)	1211	6110	1260	DNC	DNC	3337	1137	2187
$\lvert\bar{\tau}\rvert$ (Nm)	14.2	31.9	14.5	–	–	23.6	13.8	19.1

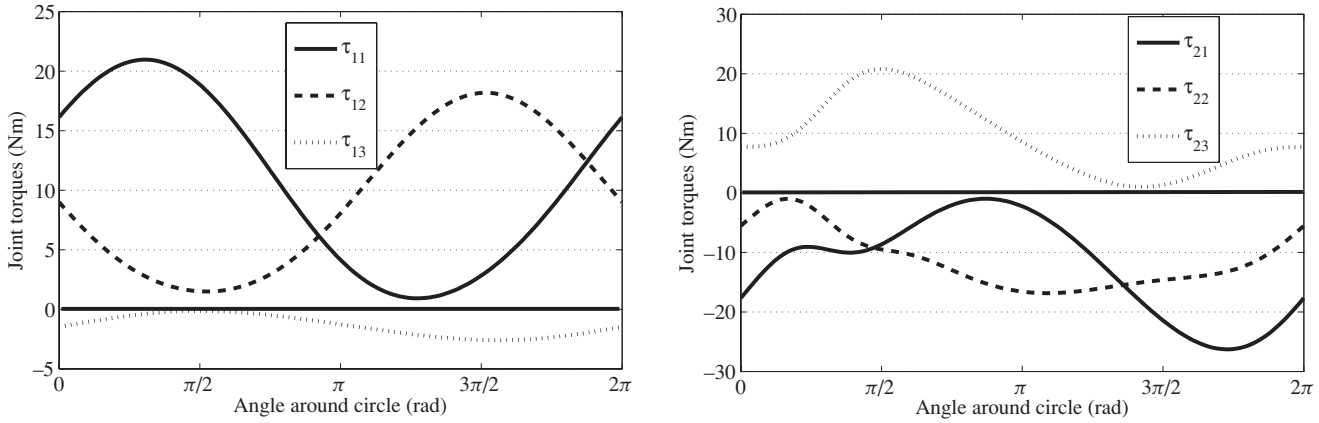

Fig. 6. 3-*RRR* manipulator optimized joint torques to follow circle trajectory using ++− combination for the base joint torques: (a) Base (1st) joint torques; (b) Elbow (2nd) joint torques.

https://doi.org/10.1017/S026357471100066X Published online by Cambridge University Press

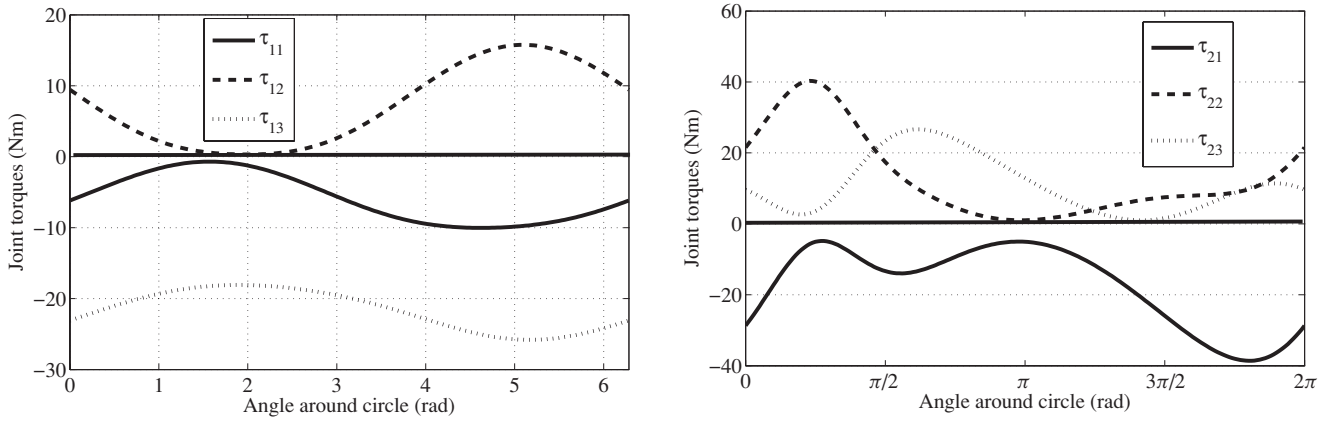

Fig. 7. 3-*RRR* manipulator optimized joint torques to follow circle trajectory using $-+-$ combination for the base joint torques: (a) Base (1st) joint torques; (b) Elbow (2nd) joint torques.

wave curves for the base joint torques do not start and finish at the same amplitude, as would be expected for a sine wave varying from 0 to 2π. The reason for this is that it is the wrench intensities of the base joints that were input as the sine wave, not the base joint torques. Since the start and end positions on the spiral are not the same, as was the case for the circle trajectory, the conversion from wrench intensities to joint torques using Eq. (3) is different.

6.6. Arc trajectory results

The method applied thus far fails if it is applied to the arc trajectory described in Section 6.1 since the ARSs of the base actuated joints almost collapse into a pencil of screws, i.e., become a 2-system (singular), when the manipulator passes through a certain point on the trajectory. This position is shown in Fig. 10. It can be observed that the ARSs of the first actuated joints of the first and second branches, which pass through the distal links, are almost aligned, and thus, the

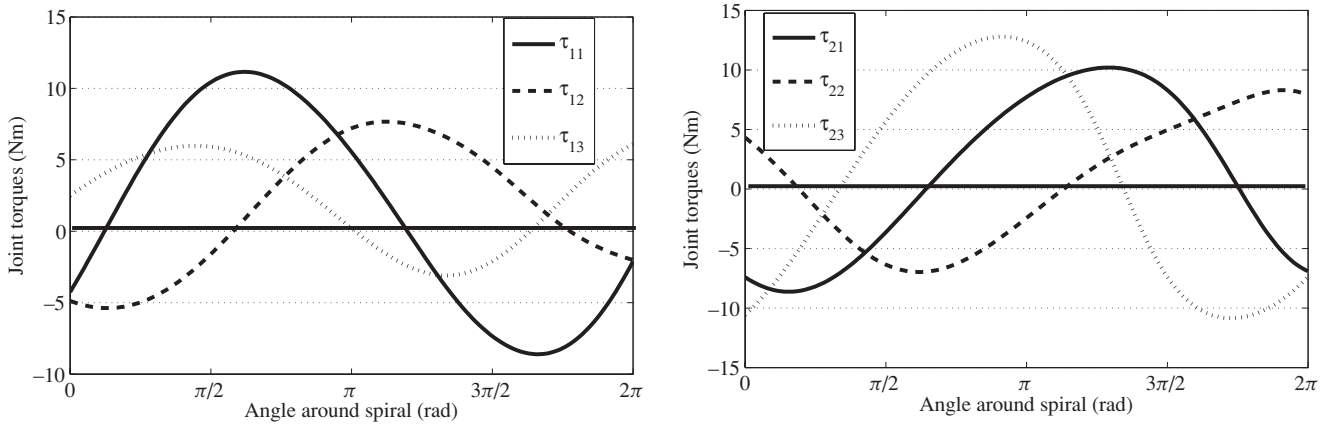

Fig. 8. 3-*RRR* manipulator joint torques to follow spiral trajectory using pseudoinverse solution: (a) Base (1st) joint torques; (b) Elbow (2nd) joint torques.

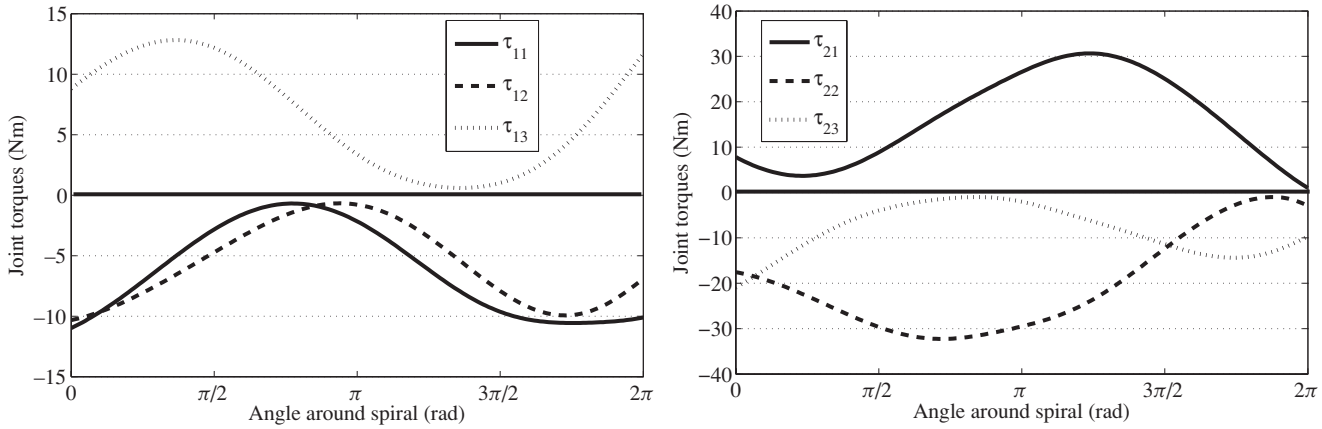

Fig. 9. 3-*RRR* manipulator optimized joint torques to follow spiral trajectory using $--+$ combination for the base joint torques: (a) Base (1st) joint torques; (b) Elbow (2nd) joint torques.

https://doi.org/10.1017/S026357471100066X Published online by Cambridge University Press

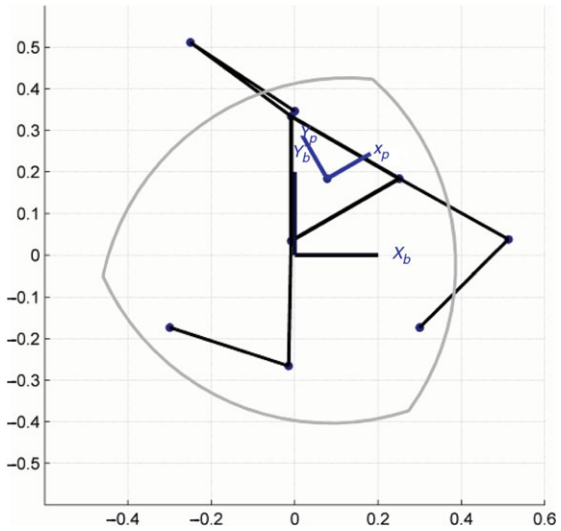

Fig. 10. (Colour online) Singular position of manipulator when following arc trajectory.

three base actuated ARSs are close to meeting at a point. In this case, matrix $[\$'_3]$ is ill-conditioned and problems occur when trying to invert it. This causes difficulties when the algorithm tries to compute Eq. (6) or Eq. (9).

To solve this problem, one can examine the static force problem, Eq. (7), for the 3-*RRR* PM. Instead of writing the equation as such, any order of the ARSs can be used. Since the first three screws produce a matrix that is almost singular, one of the ARSs of $[\$'_3]$ can be switched with one of the ARSs of the elbow actuated joints to create another matrix that is not singular. In what follows, a new matrix $[\$'_3]_{\text{new}}$ is formed by switching the order of the ARSs $\$'_{11}$ and $\$'_{21}$ of branch 1 in matrix $\$'_6$. Note that this combination was chosen to eliminate the condition described in the previous paragraph. The ARSs of the second branch could also have been chosen for switching. Note that switching the ARSs of the third branch would not be a good choice, since the ARSs of the base actuated joints of the first and second branches would still be almost aligned and the new matrix formed would also be ill-conditioned.

The new matrix formed by the switching proposed here is used in Eq. (9) to compute the nullspace basis vectors and in Eq. (14) for the particular solution. The desired values are then specified for the wrench intensity values of the elbow actuated joint of the first branch and for the base actuated joints of branches 2 and 3, i.e., w_{21}, w_{12}, and w_{13}. The compensation wrench intensities computed with Eq. (16) are then obtained for the base actuated joint of the first branch and for the elbow actuated joints of branches 2 and 3. The method described in Section 5.4 is basically followed but with different ARSs in the matrices.

The optimization algorithm was applied with the method described. A sine wave was again selected for the desired wrench intensities. It converged to a solution in six of the possible eight sign combinations for the desired wrench intensities. The optimization results are given in Table III. The trajectory was again divided into 201 points. Figure 11 presents the optimization results obtained with the $-++$ combination.

7. Discussion

Nonredundantly actuated PMs require positive and negative joint torques to follow trajectories with arbitrary applied force directions. This switching of joint torque sense will have an ill effect on payload accuracy, if there is backlash present. The addition of actuation redundancy and the use of a pseudoinverse solution decrease the joint torques required to sustain a wrench as can be seen by a comparison of Figs. 3–5. However, the pseudoinverse solution of the static force problem for the redundantly actuated 3-*RRR* PM also produces joint torques that change sign and are a cause of backlash.

Considering redundant actuation with the 3-*RRR* PM allowed the use of a nonlinear optimization routine. By exploiting a nullspace basis of the ARS matrix, a method was proposed that assures nonreversing torques for the actuated joints thus eliminating backlash. The cost of this elimination is the necessity of slightly larger torques at the elbow joints for compensation (compare Figs. 5–7, or Figs. 8 and 9).

If singular configurations are present or if the manipulator passes close to a singular configuration when following a trajectory, switching some of the ARSs allows different matrices to be constructed that are better conditioned and thus numerically stable. The method presented in Section 5.4 can then be used with different ARSs in the matrices.

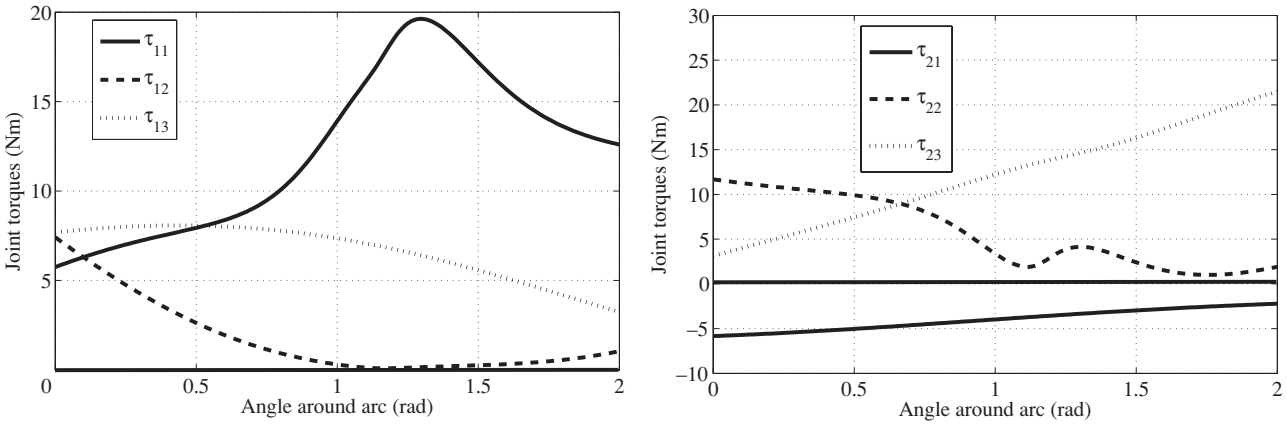

Fig. 11. 3-*RRR* manipulator optimized joint torques to follow arc trajectory using $-++$ combination for the desired joint torques: (a) Base (1st) joint torques; (b) Elbow (2nd) joint torques.

https://doi.org/10.1017/S026357471100066X Published online by Cambridge University Press

Table III. Optimization results, arc trajectory.

Combination	+++	++−	+−+	+−−	−++	−+−	−−+	−−−
OF/n_{points} (Nm)	641	1852	DNC	DNC	461	822	1050	4842
$\|\bar{\tau}\|$ (Nm)	10.3	17.6	–	–	8.8	11.7	13.2	28.4

In all the results presented, a sine wave was used to model the desired wrench intensities. This curve was chosen because of its simplicity in specifying search parameters that assure same sense outputs. With the amplitude defined by a factor less than 1 that multiplies the mean sine wave value (see Eq. (21)), same sense outputs are guaranteed. Other curves could also be used as long as proper care of the function signs is taken.

This work dealt with in-branch actuation redundancy. It should be noted that if a similar method was implemented on redundant additional branch actuation manipulators with prismatic joints, tensile forces in the prismatic joints would be analogous to a cable-driven manipulator. The prismatic joints could be replaced by a pulley mechanism.

8. Conclusion

Backlash elimination is not possible for nonredundant PMs, since there is only one solution to the static force problem. Redundantly actuated PMs have an infinite number of solutions to the inverse static force problem, thus allowing optimization to be used. The proposed method allows the specification of same sense desired torques for three of the joints. Compensation torques for the three other joints are then computed and can be obtained having the same sign by imposing constraints in the nonlinear optimization. The results presented are not necessarily the globally optimum solution that minimizes the joint torque amplitudes, but the optimized solution does guarantee nonreversing signs of all the actuated torques and thus avoids any backlash problems.

Acknowledgments

The authors would like to acknowledge the financial support of the Natural Sciences and Engineering Research Council of Canada (NSERC).

References

1. B. H. Kang, J. T.-Y. Wen, N. G. Dagalakis and J. J. Gorman, "Analysis and design of parallel mechanisms with flexure joints," *IEEE Trans. Robot.* **21**(6), 1179–1184 (2005).
2. B.-J. Yi, G. B. Chung, H. Y. Na, W. K. Kim and I. H. Suh, "Design and experiment of a 3-DOF parallel micromechanism utilizing flexure hinges," *IEEE Trans. Robot. Autom.* **19**(4), 604–612 (2003).
3. H. H. Pham and I.-M. Chen, "Optimal Synthesis for Workspace and Manipulability of Parallel Flexure Mechanism," *Proceedings of the 11th World Congress in Mechanism and Machine Science*, Tianjin, China (2004), 5p.
4. A. Müller, "Internal preload control of redundantly actuated parallel manipulators—Its application to backlash avoiding control," *IEEE Trans. Robot.* **21**(4), 668–677 (2005).
5. A. Müller and P. Maisser, "Generation and application of prestress in redundantly full-actuated parallel manipulators," *Multibody Syst. Dyn.* **18**(2), 259–275 (2007).
6. W. Wei and N. Simaan, "Design of planar parallel robots with preloaded flexures for guaranteed backlash prevention," *ASME J. Mech. Robot.* **2**, 011012 (2010).
7. C. Innocenti, "Kinematic clearance sensitivity analysis of spatial structures with revolute joints," *ASME J. Mech. Des.* **124**(1), 52–57 (2002).
8. V. Parenti-Castelli and S. Venanzi, "Clearance influence analysis on mechanisms," *Mech. Mach. Theory* **40**(12), 1316–1329 (2005).
9. A.-H. Chebbi, Z. Affi and L. Romdhane, "Prediction of the pose errors produced by joint clearance for the 3-UPU parallel robot," *Mech. Mach. Theory* **44**(9), 1768–1783 (2009).
10. C. M. Gosselin and J. Angeles, "Singularity analysis of closed-loop kinematic chains," *IEEE Trans. Robot. Autom.* **6**(3), 282–290 (1990).
11. F. Firmani and R. P. Podhorodeski, "Force-unconstrained poses for a redundantly-actuated planar parallel manipulator," *Mech. Mach. Theory* **39**(5), 459–476 (2004).
12. F. Firmani, A. Zibil, S. B. Nokleby and R. P. Podhorodeski, "Force-moment capabilities of revolute jointed planar parallel manipulators, with additional branches," *Trans. Canadian Soc. Mech. Eng.* **31**(4), 469–481 (2007).
13. A. Zibil, F. Firmani, S. B. Nokleby and R. P. Podhorodeski, "An explicit method for determining the force-moment capabilities of redundantly-actuated planar parallel manipulators," *ASME J. Mech. Des.* **129**(10), 1046–1055 (2007).
14. I. Ebrahimi, J. A. Carretero and R. Boudreau, "3-PRRR redundant planar parallel manipulator: Inverse displacement, workspace and singularity analyses," *Mech. Mach. Theory* **42**(8), 1007–1016 (2007).
15. J. P. Merlet, "Redundant parallel manipulators," *J. Laboratory Robot. Autom.* **8**(1), 17–24 (1996).
16. R. S. Ball, *Theory of screws: A Treatise on the Theory of Screws* (Cambridge University Press, New York, NY, USA, 1900).
17. K. H. Hunt, *Kinematic Geometry of Mechanisms* (Oxford University Press, Toronto, ON, Canada, 1978).
18. J. J. Craig, *Introduction to Robotics: Mechanics and Control*, 3rd ed. (Pearson Prentice Hall, Upper Saddle River, NJ, USA, 2005).
19. G. Strang, *Linear Algebra and its Applications*, 2nd ed. (Harcourt Brace, Orlando, FL, USA, 1988).
20. Wolfram MathWorld, http://mathworld.wolfram.com/LogarithmicSpiral.html (accessed Sep. 2010).
21. C. M. Gosselin, "Determination of the workspace of 6-DOF parallel manipulators," *ASME J. Mech. Des.* **112**(3), 331–336 (1990).

Appendix A. Inverse displacement solution for the *3-RRR* PM

For each of the three branches, values for the locations of the base revolute joints (B_j) on the base platform are known

$$ {}^{b}\boldsymbol{x}_{1j} = \{x_{1j}, y_{1j}\}^{\mathrm{T}} = r_{\mathrm{base}} \left\{ \cos\left(\frac{-\pi}{6} + (j-1)\frac{2\pi}{3}\right), \cos\left(\frac{-\pi}{6} + (j-1)\frac{2\pi}{3}\right) \right\}^{\mathrm{T}}, \quad j = 1, 2, 3, \tag{A1} $$

where r_{base} is the radius of the base platform.

Also known are values for the locations of the wrist joints (W_j)

$$ {}^{b}x_{3j} = \{x_{3j}, y_{3j}\}^{\mathrm{T}} = {}^{b}\boldsymbol{r}_{b-p} + {}^{b}_{p}R^{p}\boldsymbol{r}_{p-W_j}, \ j = 1, 2, 3, \tag{A2} $$

https://doi.org/10.1017/S026357471100066X Published online by Cambridge University Press

${}^{p}\boldsymbol{r}_{p-W_j}$ is the position vector from the center of the platform to joint W_j expressed in $\{\mathbf{p}\}$. Once the locations of the base and wrist joints are known for each branch, the inverse displacement solution simply becomes the elbow up or elbow down solution of a planar serial manipulator with two links that can readily be found in any elementary robotics textbook. Using the solution of ref. [15], we have

$$\cos\theta_{2j} = \frac{a_j^2 + b_j^2 - b_j e_j^2 - e_j w_j}{2 b_j e_j e_j w_j}, \quad j = 1, 2, 3, \quad \text{(A3)}$$

where $b_j e_j$ and $e_j w_j$ are the lengths between the base joints and elbow joints, and between the elbow joints and wrist joints, respectively, $a_j = x_{3j} - x_{1j}$ and $b_j = y_{3j} - y_{1j}$. Values of θ_{2j} between 0 and π are used in this work. The solutions for θ_{1j} are given by

$$\theta_{1j} = \text{atan2}(b_j, a_j) - \text{atan2}(k_{2j}, k_{1j}), \quad \text{(A4)}$$

where $k_{2j} = b_j e_j + e_j w_j \cos\theta_{2j}$ and $k_{1j} = e_j w_j \sin\theta_{2j}$.

Appendix B. The ARSs of the 3-$\underline{R}RR$, 3-$R\underline{R}R$ and 3-$\underline{RR}R$ PMs

The ARSs of the actuated base joints of the 3-$\underline{R}RR$ wrt the base frame are given by

$$\$'_{1j} = \{\cos(\theta_{1j} + \theta_{2j}), \sin(\theta_{1j} + \theta_{2j}); d_{1j}\}^{\mathrm{T}}, \quad \text{(B1)}$$

where $d_{1j} = x_{2j}\sin(\theta_{1j} + \theta_{2j}) - y_{2j}\cos(\theta_{1j} + \theta_{2j})$ with $x_{2j} = x_{1j} + b_j e_j \cos(\theta_{1j})$ and $y_{2j} = y_{1j} + b_j e_j \sin(\theta_{1j})$.

The ARSs of the actuated elbow joints of the 3-$R\underline{R}R$ wrt the base frame are given by:

$$\$'_{2j} = \left\{ \frac{x_{1j} - x_{3j}}{\text{norm}}, \frac{y_{1j} - y_{3j}}{\text{norm}}; d_{2j} \right\}^{\mathrm{T}}, \quad \text{(B2)}$$

where $\text{norm} = \sqrt{(x_{3j} - x_{1j})^2 + (y_{3j} - y_{1j})^2}$ and $d_{2j} = x_{1j}\frac{(y_{1j} - y_{3j})}{\text{norm}} - y_{1j}\frac{(x_{1j} - x_{3j})}{\text{norm}}$.

For the redundantly actuated 3-$\underline{RR}R$ PM, the ARSs consist of the ARSs given by Eqs. (B1) and (B2).

https://doi.org/10.1017/S026357471100066X Published online by Cambridge University Press